Volume 1 | Number 1 | Jan 2013 | Pages 1–100

Journal of
Materials Chemistry A

Materials for energy and sustainability
www.rsc.org/materialsA

ROYAL SOCIETY
OF CHEMISTRY

ROYAL SOCIETY
OF CHEMISTRY

www.rsc.org/materialsA

Journal Name

ARTICLE TYPE

A Functionalized Graphene Oxide and Nano Zeolitic Imidazolate Frameworks Composite as Highly Active and Reusable Catalyst for [3+3] Formal Cycloaddition Reactions

Yongyi Wei,[‡] Zhongkai Hao,[‡] Fang Zhang* and Hexing Li*

We report a facile coordination-induced growth approach to fabricate a SO_3H-functionalized graphene oxide and nanosized zeolitic imidazolate frameworks composite (ZIF-8@SO_3H-GO) in mild conditions. The interactions between the functional groups on the sheets of GO with Zn(II) ions of ZIF-8 precursor
[10] initiated the nucleation and growth of ZIF-8 on the GO and meanwhile nanosized ZIF-8 particels were well dispersed on the sheets of GO. Owing to the co-existed basic imidazole moieties from ZIF-8 and the SO_3^- and CO_2^--functional groups on the sheets and Zn^{2+} ions from ZIF-8 in this Lewis acid rich composite, it exhibited high catalytic reactivity and selectivity in [3+3] formal cycloaddition reactions that consist of two-step Knoevenagel-type condensation and electrocyclic ring-closure to give various synthetically
[15] valuable pyranyl heterocycles. Interestingly, it was especially advantageous for the large size reactants. The results indicated that it displayed 2 times higher reactivity compared to ZIF-8 nanoparticles due to the newly formed mesopores in the junctions between GO sheets and ZIF-8 nanoparticles. More importantly, it could be conveniently recovered and recycled for 10 times without loss of activity.

Introduction

[20] Metal-organic frameworks (MOFs) are ordered porous crystalline materials constituted by the metal ion nodes and the organic molecule linkers in a specific coordination number and geometry.[1] Because of large surface area, high porosity, and precisely controllable structure and functionality, MOFs have
[25] attracted enormous recent interest in heterogeneous catalysis.[2] Until now, they have been extensively used in a wide range of chemical transformations, such as acid or base catalysis,[3-4] selective oxidation,[5] asymmetric organic synthesis[6] and photocatalysis.[7] In this context, one of most promising
[30] application is the use of MOFs as solid catalysts for multistep synthesis because the versatilities in component and morphology of MOFs allow for a large extent design in the composition, configuration and dispersion of varied active species.[8] Obviously, these systems offer the significant benefits to chemical synthesis
[35] owing to the increased process intensification and sustainability, and the reduction of costs and wastes.[9] To date, some MOFs have been developed for various multistep reactions in different acid/base, oxidation/reduction, and metal-organic combination ways, including pristine MOFs,[10] organic-functionalized MOFs[11]
[40] and metal particles loading MOFs.[12] However, the existence of diffusion limitation caused by the relatively small pores in most of these reported MOFs impedes their practical usefulness in the multiple chemical transformations. Moreover, these above-mentioned MOFs have rarely been adopted to construct
[45] synthetically useful and complex molecules.[13] Therefore, the design of the novel MOFs-based solid catalyst with high

reactivity and stability for multistep synthesis still remains a big challenge.

Recently, graphene oxide (GO) with a two-dimensional sheet-
[50] like structure and the abundant functional groups provides a novel platform for the nucleation and subsequent growth of MOFs, resulting in the generation of a series of MOFs@GO hybrid nanocomposites.[14] Interestingly, these functional materials exhibited the remarkably enhanced properties compared to the
[55] individual corresponding MOFs or GO in adsorption application such as CO_2 capture and reactive adsorption of toxic gas, due to the additional pores existed in the MOFs@GO interface and the increase dispersive interactions.[15] In spite of these recent advances, there has been relatively little exploration in
[60] heterogeneous catalysis by using MOFs@GO nanocomposites, especially for multistep reactions.[16] Herein we reported for the first time the synthesis of a functionalized graphene oxide and nano-ZIF-8 composite (ZIF-8@SO_3H-GO) by a facile coordination-induced growth approach. Owing to the co-existed
[65] basic imidazoles and the abundant Lewis acidic species including the SO_3^- and CO_2^--functional groups on the sheets and Zn^{2+} ions it showed excellent catalytic reactivity and selectivity in [3+3] formal cycloaddition reactions that comprise of two-step Knoevenagel-type condensation and electrocyclic ring-closure to
[70] give a variety of synthetically valuable pyranyl heterocycles. Noted that it was especially advantageous for the large size molecules due to the newly formed mesopores in the junctions between GO sheets and ZIF-8 nanoparticles. Meanwhile, it also was easily isolated by simple filtration and reused for ten times

without significant degradation in catalytic activity.

Experimental section

1. Sample preparation

1.1 Synthesis of sulfonated graphene oxide (SO₃H-GO)

Graphene oxide (GO) was firstly prepared by the conventional Hummers method. In a typical procedure, the mixture of 1.0 g natural graphite powder and 1.0 g anhydrous $NaNO_3$ was added slowly into 40 ml concentrated H_2SO_4 (98%) under an ice bath. After continuous stirring for 2.0 h, 5.0 g $KMnO_4$ was gradually added into the mixture. Next, the mixture temperature was increased to 35°C and allowed to stir for another 24 h. Then, after the temperature was adjusted to 60°C, 100 ml 0.50 mol/L H_2SO_4 aqueous solution was added. After stirring for 2.0 h, the temperature continued to increase to 95°C. Subsequently, 100 ml 30% H_2O_2 aqueous solution and 1000 ml H_2O were successively added into the mixture. After stirring for 0.5 h, the solid sample was thoroughly washed with 0.50 mol/L HCl aqueous solution and water for five times. The obtained graphene oxide was collected by centrifugation and vacuum drying at 60°C for 12 h. After that, 0.50 g GO was introduced into 10 ml chlorosulfonic acid (HSO_3Cl) under nitrogen atmosphere and then sonicated for 0.5 h. After stirring for 12 h, the mixture was added into 500 ml deionized water and allowed to stir for 1.0 h. The obtained product was separated by centrifugation, washed with ethanol and water, and dried in vacuum at 80°C for 10 h.

1.2 Fabrication of graphene oxide-nano zeolitic imidazolate frameworks composite (ZIF-8@SO₃H-GO)

Firstly, a certain amount of GO was dispersed into 10 ml 2-methylimidazole aqueous solution (3.5 mol/L) at 30°C and sonicated for 0.5 h. Then, 1.0 ml $Zn(NO_3)_2$ aqueous solution (0.50 mol/L) was dropwise added into the mixture under magnetically stirring and afterward allowed to continuous stir for 12 h. After centrifugation, the solid sample was washed by imidazole buffer solution and ethanol for three times to thoroughly remove the uncoordinated Zn ion and 2-methylimidazole. Finally, the product was dried at 80°C in vacuum for 12 h. The final catalyst could be defined as ZIF-8@SO₃H-GO-1, ZIF-8@SO₃H-GO-2 and ZIF-8@SO₃H-GO-3, corresponding to 50 mg, 100 mg and 200 mg GO used in the initial mixture, respectively.

1.3 Synthesis of nano zeolitic imidazolate frameworks (ZIF-8)

1.0 ml $Zn(NO_3)_2$ aqueous solution (0.50 mol/L) was dropwise added into 10 ml 2-methylimidazole aqueous solution (3.5 mol/L) at 30°C under magnetically stirring. After stirring for 12 h, the white powder was collected by centrifugation and washed by deionized water and ethanol for three times, dried in vacuum at 80°C for 6.0 h.

2. Characterization

The nitrogen, carbon and sulfur contents were calculated in a Vario EL III Elemental analysis analyzer. The surface electronic states were analyzed by X-ray photoelectron spectroscopy (XPS, Perkin-Elmer PHI 5000C ESCA). All the binding energy values were calibrated by using $C_{1S} = 284.6$ eV as a reference. X-ray

diffractions (XRD) were performed on a Rigaku D/MAX B diffraction system with Cu Kα radiation. N_2 adsorption-desorption isotherms were obtained on a Micromeritics ASAP2020 analyzer. Transmission electron microscopy (TEM) images were obtained on a JEOL JEM2011 electron microscope.

3. Activity Test

In a typical procedure of [3+3] formal cycloaddition reaction, 1.0 mmol 1,3-cyclohexanedione, 1.0 mmol 3-methyl-2-butenal, 50 mg solid catalyst and 5.0 ml CH_2Cl_2 were mixed and allowed to stir at 20°C for 24 h. The product was extracted with ethyl acetate, followed by analysis on a high performance liquid chromatography analyzer (HPLC, Agilent 6410 series Triple Quad) equipped with an Agilent C18 column. The reaction conversion was calculated based on the consumption of 3-methyl-2-butenal and the selectivity was determined by the yield of the achieved pyranyl heterocycle product.

In order to determine the catalyst recyclability, ZIF-8@SO₃H-GO-2 was centrifuged after each run of [3+3] formal cycloaddition reaction with 1,3-cyclohexanedione and 3-methyl-2-butenal as the reactants and the clear supernatant liquid was decanted slowly. The residual solid catalyst was washed thoroughly with toluene and dichloromethane, followed by vacuum drying at 80°C for 6.0 h. Then, the catalyst was re-used with a fresh charge of solvent and reactants for subsequent recycle runs under the same reaction conditions.

Results and discussion
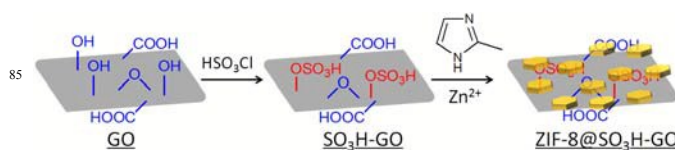
Scheme 1 Schematic synthesis of ZIF-8@SO₃H-GO composites.

The synthesis of graphene oxide and nano zeolitic imidazolate frameworks composite (ZIF-8@SO₃H-GO) was illustrated in Scheme 1. Briefly, GO was prepared according to previously reported Hummers method.[17] Then, chlorosulfuric acid (HSO_3Cl) was chosen to react with GO to afford SO₃H-functionalized GO (SO₃H-GO). Next, SO₃H-GO was admitted into a mixture of 2-methylimidazole and $Zn(NO_3)_2$ aqueous solution. The coordination interactions of the SO_3^- and COO^- ions on the sheets of GO with Zn ions initiated the growth of ZIF-8 nanoparticles, leading to the formation of ZIF-8@SO₃H-GO nanocomposite. In parallel, ZIF-8 nanoparticles were also synthesized in aqueous solution by using the same precursors.

Elemental analysis revealed that the sulfur content in GO sample was only 0.105 wt.% (Table S1). Also, S2p XPS spectrum (Figure S1) revealed that no apparent signal of sulfur element could be detected, confirming the negligible sulfur specie in the GO sample due to the efficient washing work-up treatment.[18] For comparison, the sulfur amount was found with 1.75 wt.% in SO₃H-GO (Table S1). FTIR spectra (Figure S2) showed that SO₃H-GO exhibited an additional peak at 1090 cm⁻¹ characteristic of the stretching vibration of S=O bond in comparison with GO.[19] In addition, S2p XPS spectrum (Figure 1a)

of SO$_3$H-GO displayed an obvious peak at 168.6 eV associated with the S-O bond.[20a] These results indicated the successful modification of SO$_3$H groups on the GO. Moreover, C1s spectrum of SO$_3$H-GO (Figure 1b) revealed that the peak at 286.9 eV characteristic of C-OH and C-O-C moieties almost completely disappeared while the peaks at 284.7 and 289.1 eV corresponding to sp^2 C-C bonding and carboxylic acid group remained almost the same with GO,[20b] suggesting the incorporation of SO$_3$H-groups on the GO *via* a possible esterification reaction between the surface hydroxyl groups (OH-) and HSO$_3$Cl.[19a] Furthermore, FTIR spectrum of the representative ZIF-8@SO$_3$H-GO-2 (Figure S2) exhibited the typical ZIF-8 absorption peaks at 990, 1585 and 2960 cm^{-1} corresponding to C-N stretch, C=N stretch and aliphatic C-H stretch of imidazole groups, respectively.[21] In addition, N1s XPS spectrum of ZIF-8@SO$_3$H-GO-2 (Figure 1c) displayed the almost same peak at 398.7 eV indicative of imidazole moieties with ZIF-8 nanoparticles,[22] demonstrating the effective nucleation and growth of ZIF-8 on the GO. Interestingly, S2p XPS spectrum (Figure 1a) revealed the complete disappearance of S-O bond signal for ZIF-8@SO$_3$H-GO-2 composite. Also, C1s XPS spectrum of ZIF-8@SO$_3$H-GO-2 (Figure 1b) showed that the peak at 289.1 eV attributed to carboxylic acid group also disappeared. This phenomenon suggested that both SO$_3^-$ and COO$^-$ ions initiated the growth of ZIF-8 on the sheets of GO, thereby these functional groups were covered by ZIF-8 after the formation of ZIF-8@SO$_3$H-GO composite.
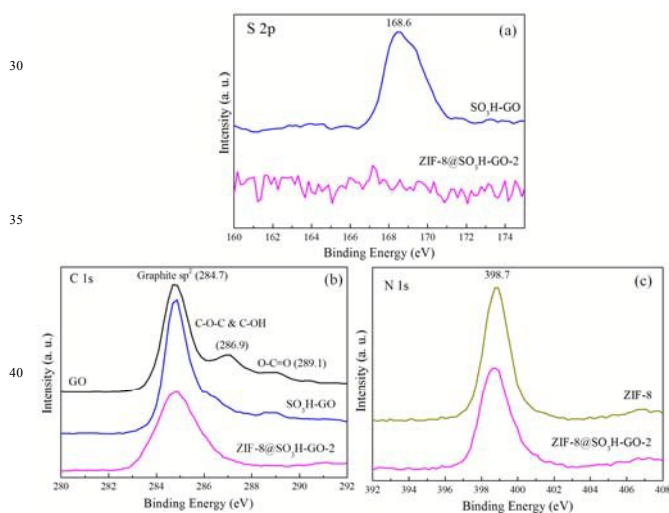
Figure 1. S2p XPS spectra (a) of SO$_3$H-GO and ZIF-8@SO$_3$H-GO-2, C1s XPS spectra (b) of GO, SO$_3$H-GO and ZIF-8@SO$_3$H-GO-2 and N1s XPS spectra (c) of ZIF-8 and ZIF-8@SO$_3$H-GO-2.

XRD spectra (Figure 2a) showed that the major diffraction peak at 2θ = 10.2° assigned to (001) plane in GO almost completely disappeared and changed to a broad peak in SO$_3$H-GO. In combination with its TEM image (Figure S3), these results revealed that the sheets of SO$_3$H-GO were efficiently exfoliated with single or several layers, providing a suitable two-dimensional support to attach the nanoparticles on its sheets.[23] Accordingly, XRD spectra of these ZIF-8@SO$_3$H-GO composites exhibited the similar well resolved diffraction peaks to those of ZIF-8 nanoparticles, evidently identifying the generation of ZIF-8 with the crystalline size on the nanoscale.[24] The intensities of diffraction peaks were gradually decreased with the increase amounts of GO in the initial solution, which was maybe attributed to the reduced ZIF-8 size and the increased amount of low crystallinity GO. Additionally, N$_2$ sorption isotherms of different samples were shown in Figure 2b. Only a very low amount of N$_2$ molecules was adsorbed on the GO. Meanwhile, ZIF-8 displayed the type I adsorption-desorption isotherm, indicating its microporous structure.[25] The shape of the isotherms for all the ZIF-8@SO$_3$H-GO composites was quite similar to ZIF-8. However, the additional small hysteresis loops at high relative pressure around p/p$_0$ = 0.47-1.0 can be seen in ZIF-8@SO$_3$H-GO-1 and ZIF-8@SO$_3$H-GO-2. It was probably assigned to the formation of mesopores that existed in the junctions between ZIF-8 and GO surface for ZIF-8@SO$_3$H-GO composites.[26] As shown in Table 1, the average pore sizes of ZIF-8@SO$_3$H-GO-1 and ZIF-8@SO$_3$H-GO-2 that calculated from their adsorption branches were 1.9 and 2.1 nm, further confirming the newly generated mesopores. Moreover, the specific surface areas and pore volumes of ZIF-8@SO$_3$H-GO samples were gradually decreased with the increasing GO percentages in these composites (Table 1), which can be explained by the increasing proportion of nonporous GO in the composites.
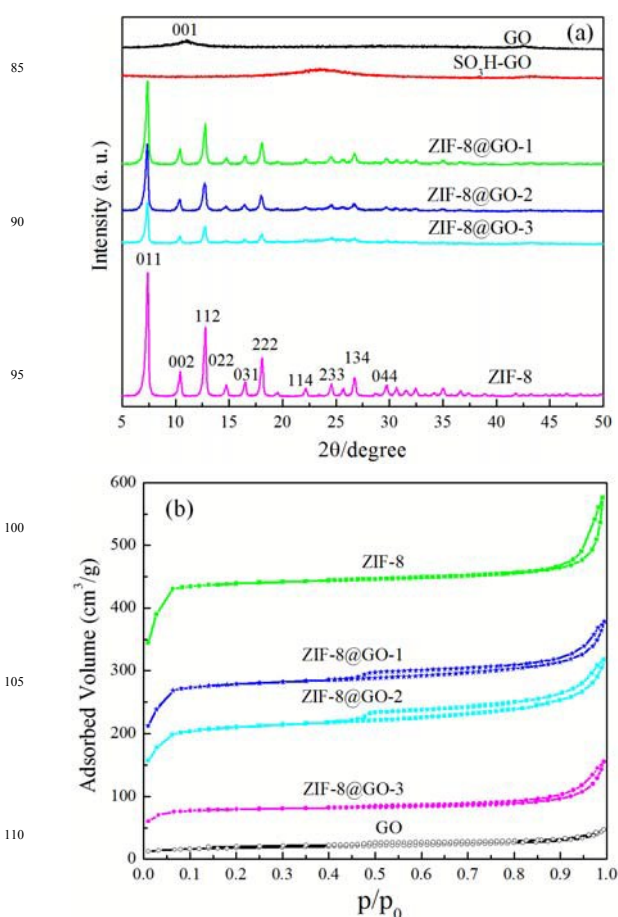

Figure 2. XRD spectra (a) and N$_2$ adsorption-desorption isotherm (b) of different samples.

Table 1. Textural parameters of different samples.

Sample	BET (m²/g)	Pore Volume (cm³/g)	Pore Size (nm)
GO	58 ± 4	0.05	/
SO₃H-GO	60 ± 5	0.07	/
ZIF-8	1315 ± 39	0.76	/
ZIF-8@ SO₃H-GO-1	842 ± 26	0.52	1.9
ZIF-8@ SO₃H-GO-2	643 ± 21	0.43	2.1
ZIF-8@ SO₃H-GO-3	242 ± 8	0.18	/

The morphologies of ZIF-8@SO₃H-GO composites were indicated by transmission electron microscopy (TEM). In the absence of GO, the as-made ZIF-8 nanoparticles displayed the approximate rhombohedral shape with the particle size in the range of 80 to 100 nm (Figure 3a). In comparison, ZIF-8 particles with around 100 nm size were randomly distributed on the GO layers in ZIF-8@SO₃H-GO-1 (Figure 3b). However, for ZIF-8@SO₃H-GO-2, most of ZIF-8 particles with about 80 nm size and some smaller particles with 20-30 nm size were densely laid on the surface (Figure 3c). However, ZIF-8 particles with ca. 80 nm size were sporadically dispersed in the stacked interlays of ZIF-8@SO₃H-GO-3 (Figure 3d). The drastic morphological differences highlighted the critical role of GO as a novel support for mediating the growth of ZIF-8. It was also important to note that the decreased amount of GO (50 mg) caused the bigger ZIF-8 size probably due to the less coordination sites while the increased amount of GO (200 mg) induced the irregular distribution maybe owing to the serious accumulation of GO sheets.[14b, g]
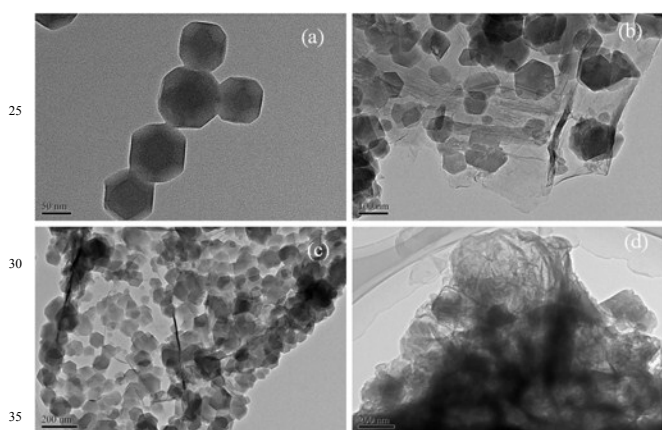
Figure 3. TEM images of ZIF-8 (a) and ZIF-8@SO₃H-GO (b-d) composites.

[3+3] formal cycloaddition reaction is the important tool for constructing piperidine ring, which is one of the most common structural subunits in natural products and biologically active compounds. It consists of a Knoevenagel-type condensation followed by a reversible 6π-electron electrocyclic ring-closure.[27] In this regard, we firstly employed [3+3] formal cycloaddition reaction between 1,3-cyclohexanedione and 3-methyl-2-butenal as a model reaction to evaluate the catalytic efficiencies of ZIF-8@SO₃H-GO composites. As summarized in Table 2, the blank experiment couldn't give any products and SO₃H-GO also showed the low conversion (40%). ZIF-8 nanoparticles obtained the good conversion with 81%. It was worthy to mention that all the ZIF-8@SO₃H-GO composites promoted this reaction with the enhanced catalytic reactivity and ZIF-8@SO₃H-GO-2 gave the excellent result with 94% conversion. This phenomenon suggested that the basic imidazole moieties and the SO₃⁻ and CO₂⁻-functional groups and Zn²⁺ ions in these Lewis acid rich composites cooperatively catalyzed this reaction.[13] The inferior reactivity of ZIF-8@SO₃H-GO-1 could be attributed to the bigger ZIF-8 particle size and the lowest catalytic efficiency of ZIF-8@SO₃H-GO-3 could be assigned to the reduced accessible active sites. Interestingly, the physical mixture of SO₃H-GO and ZIF-8 still achieved the unsatisfactory yield (76%), probably due to the increased mass transfer resistance between two different solid catalysts, especially in stirring reaction conditions. Moreover, the commonly used homogeneous Lewis acids AlCl₃ was chosen for comparison.[28] It displayed the similar conversion (97%) with ZIF-8@SO₃H-GO-2, further confirming the excellent catalytic performances of ZIF-8@SO₃H-GO composite.
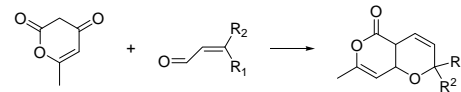
Table 2. Catalytic properties of different catalysts in [3+3] formal cycloaddition reactions between 1,3-cyclohexanedione and α,β-unsaturated aldehydes.[a]

Catalyst	Aldehyde	Product	Conv. (%)	Sel. (%)
ZIF-8@SO₃H-GO-1			90	99
ZIF-8@SO₃H-GO-2			94	99
ZIF-8@SO₃H-GO-3			85	99
SO₃H-GO			40	99
ZIF-8			81	99
SO₃H-GO + ZIF-8[b]			77	99
AlCl₃[c]			97	99
ZIF-8@SO₃H-GO-1			59	95
ZIF-8@SO₃H-GO-2			71	98
ZIF-8@SO₃H-GO-3			47	91
SO₃H-GO			33	98
ZIF-8			37	90
SO₃H-GO + ZIF-8[b]			42	97

[a] Reaction conditions: 50 mg ZIF-8@SO₃H-GO, ZIF-8 or SO₃H-GO, 1.0 mmol 1,3-cyclohexanedione, 1.0 mmol aldehyde, 5.0 mL of CH₂Cl₂, T = 20°C, t = 24 h. [b] 30 mg GO + 20 mg ZIF-8. [c] 13.3 mg AlCl₃.

To further explore the advantage of ZIF-8@SO₃H-GO, we chosen 3-(9-anthryl)acrylaldehyde with much large molecular size as the reactant (Table 2). ZIF-8 exhibited the significant decreased conversion (37%) because its small micropore was difficult to allow the effective diffusion for large molecule. Meanwhile, the other byproduct was formed due to the self-condensation of α,β-unsaturated aldehydes, leading to the reduced selectivity (90%).[29] Noted that ZIF-8@SO₃H-GO-2 displayed the good conversion (71%) and excellent selectivity (98%). As the result, the yield of ZIF-8@SO₃H-GO-2 was 2 times higher than that of ZIF-8. This remarkable enhancement could be explained that the newly formed mesopores in the junctions between GO sheets and ZIF-8 nanoparticles were readily accessible to the reactants with the decreased mass transfer resistance.[30]

Table 3. Catalytic properties of ZIF-8@SO$_3$H-GO-2 and ZIF-8 in [3+3] formal cycloaddition reactions between 4-pyran-3,6-dione and α, β-unsaturated aldehydes.[a]

| Catalyst	Aldehyde	Product	Conv. (%)	Sel. (%)
ZIF-8@GO-2			72	99
ZIF-8			54	99
ZIF-8@GO-2			63	99
ZIF-8			41	99
ZIF-8@GO-2			51	99
ZIF-8			26	99
ZIF-8@GO-2			40	99
ZIF-8			21	99
ZIF-8@GO-2			31	93
ZIF-8			15	91

[a] Reaction conditions: 50 mg ZIF-8@SO$_3$H-GO-2 or ZIF-8, 1.0 mmol 4-pyran-3,6-dione, 1.0 mmol aldehyde, 5.0 mL of CH$_2$Cl$_2$, T = 20°C, t = 24 h.

(ZIF-8@SO$_3$H-GO)

A = Acids: SO$_3^-$, CO$_2^-$ and Zn^{2+}
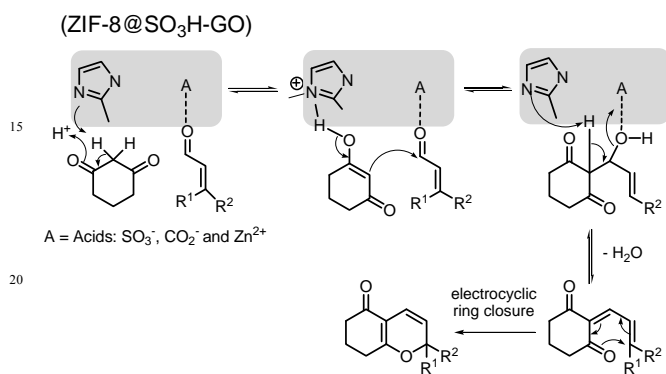
Scheme 2 A possible cooperative catalytic mechanism of ZIF-8@SO$_3$H-GO for [3+3] formal cycloaddition reaction.

Encouraged by these promising results, we next investigated the capability of ZIF-8@SO$_3$H-GO-2 catalyst to the other heterocycle synthesis (Table 3). For 4-pyran-3,6-dione participated [3+3] formal cycloaddition reactions, similar benefits were also achieved with superior reactivity for ZIF-8@SO$_3$H-GO-2. It displayed the higher catalytic efficiencies in all the α, β-unsaturated aldehydes compared with ZIF-8. Noted that it showed the same trend for the large size molecules. For example, for these aromatic aldehydes, it exhibited at least 2.0 times improved conversion compared to ZIF-8 nanoparticles. These results clearly demonstrated the generality of the strategy for the use of ZIF-8@SO$_3$H-GO nanocomposites for the multistep synthesis of structurally diverse and functionalized molecules. On the basis of these results, a plausible cooperative mechanism for ZIF-8@SO$_3$H-GO catalyzed [3+3] formal cycloaddition reaction was proposed (Scheme 2). The SO$_3^-$ and CO$_2^-$-functional groups on the sheets and Zn^{2+} ions from ZIF-8 in this Lewis acid rich composite activated α, β-unsaturated aldehyde through hydrogen bonding to the carbonyl group, while the neighbouring imidazole groups of ZIF-8 on the sheets of GO attacked the dione. Then,

both the Lewis acids and base moieties stabilized the intermediate and generated the condensation product after eliminating one molecule water. After the electrocyclic ring closure process, ZIF-8@SO$_3$H-GO composite gave the final pyranyl heterocycle product.[31]
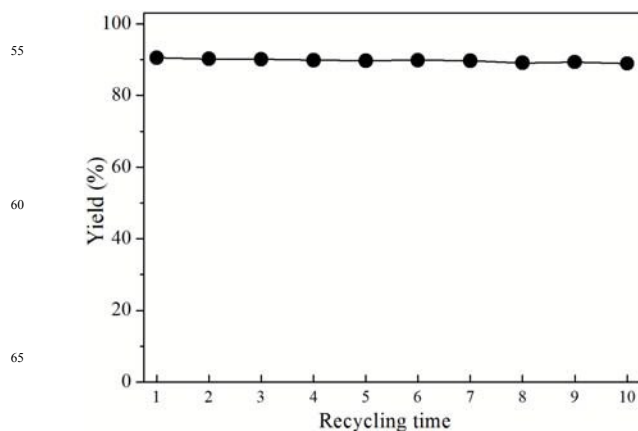
Figure 4. The recycling test of ZIF-8@SO$_3$H-GO-2 in [3+3] formal cycloaddition reaction between 1,3-cyclohexanedione and 3-methyl-2-butenal. Reaction conditions are given in Table 2.

Furthermore, we examined the durability of ZIF-8@SO$_3$H-GO-2 in [3+3] formal cycloaddition reaction with 1,3-cyclohexanedione and 3-methyl-2-butenal as the reactants. No significant decrease could be found in the yield of 7,8-dihydro-2,2-dimethyl-2H-chromen-5(6H)-one after being used repetitively for ten times (Figure 4). Elemental analysis (Table S1) revealed that after being used for ten times, the nitrogen content in the recycled ZIF-8@SO$_3$H-GO-2 remained almost the same (13.2 wt.%). Meanwhile, TEM image of the recycled ZIF-8@SO$_3$H-GO-2 confirmed almost no remarkable change in the structure before and after reuse (Figure S4). These results were in good agreement with an excellent retention of the activity of ZIF-8@SO$_3$H-GO-2 catalyst.

Conclusions

In summary, we have synthesized a functionalzied graphene oxide and nano ZIF-8 composite *via* a facile coordination-induced approach. With high dispersed basic ZIF-8 nanoparticles and the rich Lewis acids in this composite, it showed the cooperative catalytic behavior in [3+3] formal cycloaddition reactions and obtained high catalytic reactivity and selectivity for a wide range of the reactants. It is worth mentioning that it was advantageous for the large size molecules due to the diminished diffusion limitation derived from the added mesopores in the junctions between GO sheets and ZIF-8 nanoparticles. Meanwhile, it can be recycled and reused at least 10 times without loss of activity. The presented strategy could be further extended to develop more robust MOFs@GO nanocomposites for multistep synthesis to synthetically valuable and complex molecules.

Acknowledgements

Notes and references

The Education Ministry Key Lab of Resource Chemistry and Shanghai Key Laboratory of Rare Earth Functional Materials, Shanghai Normal University, Shanghai 200234, P. R. China. Fax: 86-21 6432 2272; Tel: 86-21 6432 2272; E-mail: zhangfang@shnu.edu.cn; HeXing-Li@shnu.edu.cn

† Electronic Supplementary Information (ESI) available: [Experimental section,]. See DOI: 10.1039/b000000x/

‡ These authors contributed equally to this work.

1 (a) T. Zhang, W. Lin, *Chem. Soc. Rev.*, 2014, **43**, 5982; (b) A. Dhakshinamoorthy, H. García, *Chem. Soc. Rev.*, 2014, **43**, 5750; (c) M. P. Suh, H. J. Park, T. K. Prasad, D. W. Lim, *Chem. Rev.*, 2012, **112**, 782; (d) T. A. Makal, J. R. Li, W. Lu, H. C. Zhou, *Chem. Soc. Rev.*, 2012, **41**, 7761; (e) W. M. Xuan, C. F. Zhu, Y. Liu, Y. Cui, *Chem. Soc. Rev.*, 2012, **41**, 1677.

2 (a) F. L. i Xamena, J. Gascon, *Metal Organic Frameworks as Heterogeneous Catalysts*, Royal Society of Chemistry, Cambridge, 2013; (b) J. Gascon, A. Corma, F. Kapteijin, F. L. i Xamena, *ACS Catal.*, 2014, **4**, 361; (c) A. Dhakshinamoorthy, M. Opanasenko, J. Čejka, H. García, *Catal. Sci. Technol.*, 2013, **3**, 2509; (d) A. Dhakshinamoorthy, A. M. Asiri, H. García, *Chem. Soc. Rev.*, 2015, **44**, 1922; (e) A. Corma, H. García, F. L. i Xamena, *Chem. Rev.*, 2010, **110**, 4606; (f) A. Schejn, A. Aboulaich, L. Balan, V. Falk, J. Lalevée, G. Medjahdi, L. Aranda, K. Mozet, R. Schneider, *Catal. Sci. Technol.*, 2015, **5**, 1829; (g) H. Zhou, X. Q. Liu, J. Zhang, X. F. Yan, Y. J. Liu, A. H. Yuan, *Int. J. Hydrogen Energy*, 2014, **5**, 2160; (h) J. Zhang, X. Q. Liu, H. Zhou, X. F. Yan, Y. J. Liu, A. H. Yuan, *RSC Adv.*, 2014, **4**, 28908.

3 J. Y. Lee, O. K. Farha, J. Roberts, K. A. Scheidt, S. T. Nguyen, J. T. Hupp, *Chem. Soc. Rev.*, 2009, **38**, 1450.

4 J. W. Liu, L. F. Chen, H. Cui, J. Y. Zhang, L. Zhang, C. Y. Su, *Chem. Soc. Rev.*, 2014, **43**, 6011.

5 K. Leus, Y. Y. Liu, P. V. D. Voort, *Catal. Rev.: Sci. Eng.*, 2014, **56**, 1.

6 (a) L. Q. Ma, C. Abney, W. B. Lin, *Chem. Soc. Rev.*, 2009, **38**, 1248; (b) Y. Liu, W. M. Xuan, Y. Cui, *Adv. Mater.*, 2010, **22**, 4112; (c) M. Y. Yoon, R. Srirambalaji, K. Kim, *Chem. Rev.*, 2012, **112**, 1196.

7 (a) C. Wang, Z. G. Xie, K. E. deKrafft, W. B. Lin, *J. Am. Chem. Soc.*, 2011, **133**, 13445; (b) A. Fateeva, P. A. Chater, C. P. Ireland, A. A. Tahir, Y. Z. Khimyak, P. V. Wiper, J. R. Darwent, M. J. Rosseinsky, *Angew. Chem. Int. Ed.*, 2012, **51**, 7440.

8 A. Dhakshinamoorthy, H. García, *ChemSusChem*, 2014, **7**, 2392.

9 M. Climent, A. Corma, S. Iborra, *Chem. Rev.*, 2011, **111**, 1072.

10 S. Rostamnia, H. Xin, N. Nouruzi, *Microporous Mesoporous Mater.*, 2013, 179, 99

11 (a) R. Siriambalaji, S. Hong, R, Natarajan, M. Y. Yoon, R. Hota, Y. Kim, Y. H. Ko, K. Kim, *Chem. Commun.*, 2012, **48**, 11650; (b) D. K. Wang, Z. H. Li, *Catal. Sci. Technol.*, 2015, **5**, 1623; (c) T. Toyao, M. Saito, Y. Horiuchi, M. Matsuoka, *Catal. Sci. Technol.*, 2014, **4**, 625; (d) Y. R. Lee, Y. M. Chung, W. S. Ahn, *RSC Adv.*, 2014, **4**, 23064; (e) F. Vermoortele, R. Ameloot, A. Vimont, C. Serre, D. D. Vos, *Chem. Commun.*, 2011, **47**, 1521.

12 (a) M. T. Zhao, K. Deng, L. C. He, Y. Liu, G. D. Li, H. J. Zhao, Z. Y. Tang, *J. Am. Chem. Soc.*, 2014, **136**, 1738; (b) T. Ishida, M. Nagaoka, T. Akita, M. Haruta, *Chem. Eur. J.*, 2008, **14**, 8456; (c) Y. Y. Pan, B. Z. Yuan, Y. W. Li, D. H. He, *Chem. Commun.*, 2010, **46**, 2280.

13 F. Zhang, Y. Y. Wei, X. T. Wu, H. Y. Jiang, W. Wang, H. X. Li, *J. Am. Chem. Soc.*, 2014, **136**, 13963.

14 (a) D. Bradashaw, A. Garai, J. Huo, *Chem. Soc. Rev.*, 2012, **41**, 2344; (b) C. Petit, T. J. Bandosz, *Adv. Mater.*, 2009, **21**, 4753; (b) X. Zhou, W. Y. Huang, J. Shi, Z. X. Zhao, Q. B. Xia, Y. W. Li, H. H. Wang, Z, Li, *J. Mater. Chem. A*, 2014, **2**, 4722; (c) J. W. Liu, Y. Zhang, X. W. Chen, J. H. Wang, *ACS Appl. Mater. Interfaces*, 2014, **6**, 10196; (d)

D. Li, L. Qiu, K. Wang, Y. Zeng, D. Li, T. Williams, Y. Huang, M. Tsapatsis, H. T. Wang, *Chem. Commun.*, 2012, **48**, 2249; (e) X. Huang, B. Zheng, Z. D. Liu, C. L. Tan, J. Q. Liu, C. L. Tan, J. Q. Liu, B. Chen, H. Li, J. Z. Chen, X. Zhang, Z. X. Fan, W. N. Zhang, Z. Guo, F. W. Huo, Y. H. Yang, L. H. Xie, W. Huang, H. Zhang, *ACS Nano*, 2014, **8**, 8695; (f) A. S. Huang, Q. Liu, N. Y. Wang, Y. Q. Zhu, J. Caro, *J. Am. Chem. Soc.*, 2014, **136**, 14686; (g) R. Kumar, K. Jayaramulu, T. K. Maji, C. N. R. Rao, *Chem. Commun.*, 2013, **49**, 4947; (h) I. Ahmed, N. A. Khan, S. H. Jhung, *Inorg. Chem.*, 2013, 52, 14155.

15 (a) C. Petit, T. J. Bandosz, *Adv. Funct. Mater.*, 2011, **21**, 2108; (b) S. Liu, L. X. Sun, F. Xu, J. Zhang, C. L. Jiao, F. Li, Z. B. Li, S. Wang, Z. Q. Wang, X. Jiang, H. Y. Zhou, L. N. Yang, C. Schick, *Energy Environ. Sci.*, 2013, **6**, 818.

16 (a) M. Jahan, Z. L. Liu, K. P. Loh, *Adv. Funct. Mater.*, **2013**, *23*, 5363; (b) D. D. Zu, L. Lu, X. Q. Liu, D. Y. Zhang, L. B. Sun, *J. Phys. Chem. C*, 2014, **118**, 19910; (c) X. Qiu, X. Wang, Y. W. Li, *Chem. Commun.*, 2015, **51**, 3874.

17 W. Zhang, S. Wang, J. Ji, Y. Li, G. Zhang, F. Zhang, X. Fan, *Nanoscale*, 2013, **5**, 6030.

18 (a) D. R. Dreyer, A. D. Todd, C. W. Bielawski, *Chem. Soc. Rev.*, 2014, **43**, 5288; (b) A. Dimiev, D. V. Kosynkin, L. B. Alemany, P. Chaguine, J. M. Tour, *J. Am. Chem. Soc.*, 2012, **134**, 2815; (c) S. Eigler, C. Dotzer, F. Hof, W. Bauer, A. Hirsch, *Chem. Eur. J.*, 2013, **19**, 9490.

19 (a) M. Hasanzadeh, N. Shadjou, *J. Nanosci. Nanotechnol.*, 2013, **13**, 4909; (b) J. O. Iroh, C. Williams, *Synth. Met.*, 1999, **99**, 1.

20 (a) F. J. Liu, J. Sun, L. F. Zhu, X. J. Meng, C. Z. Qi, F. S. Xiao, *J. Mater. Chem.*, 2012, **22**, 5495; (b) C. F. Yuan, W. F. Chen, L. F. Yan, *J. Mater. Chem.*, 2012, **22**, 7456.

21 Ma. J. C. Ordoñez, K. J. Balkis Jr., J. P. Ferraris, I. H. Musselman, *J. Membr. Sci.*, 2010, **361**, 28.

22 C. Chizallet, S. Lazare, D. Bazer-Bachi,; F. Bonnier, V. Lecocq, E. Soyer, A. A. Quoineaud, N. Bats, *J. Am. Chem. Soc.*, 2010, **132**, 12365.

23 D. W. Wang, F. Li, J. P. Zhao, W. C. Ren, Z. G. Chen, J. Tan, Z. S. Wu, L. Gentle, G. Q. Lu, H. M. Cheng, *ACS Nano*, 2009, **3**, 1745.

24 Y. C. Pan, Y. Y. Liu, G. F. Zeng, L. Zhao, Z. P. Lai, *Chem. Commun.*, 2011, **47**, 2071.

25 K. S. Park, Z. Ni, A. P. Côte, J. Y. Choi, R. Huang, F. J. Uribe-Romo, H. K. Chae,; M. O'Keeffe, O. M. Yaghi, *Proc. Natl. Acad. Sci. U.S.A.*, 2006, **103**, 10186.

26 D. D. Zu, L. Lu, X. Q. Liu, D. Y. Zhang, L. B. Sun, *J. Phys. Chem. C*, 2014, **118**, 19910.

27 G. S. Buchanan, J. B. Feltenberger, R. P. Hsung, *Curr. Org. Synth.*, 2010, **7**, 363.

28 A. V. Kurdyumov, N. Lin, R. P. Hsung, G. C. Gullickson, K. P. Cole, N. Sydorenko, J. J. Swidorski, *Org. Lett.*, 2006, **8**, 191.

29 C. Burstein, F. Glorius, *Angew. Chem. Int. Ed.*, 2004, **43**, 6205.

30 C. L. Su, K. P. Loh, *Acc. Chem. Res.*, 2013, **46**, 2275.

31 E. L. Margelefsky, R. K. Zeidan, M. E. Davis, *Chem. Soc. Rev.*, 2008, **37**, 1118.

Graphic Abstract

ZIF-8@SO$_3$H-GO

A SO$_3$H-functionalized graphene oxide and nano ZIF-8 composite was an efficient catalyst for [3+3] formal cycloaddition reactions to pyranyl heterocycles.